Received: 28 December 2021 | Revised: 7 March 2022 | Accepted: 2 April 2022 | Published on: 13 April 2022

DOI: 10.1002/joc.7640

International Journal of Climatology RMetS

RESEARCH ARTICLE

How do snow cover fraction change and respond to climate in Altai Mountains of China?

Shen Qin[1] | **Pengfeng Xiao**[1,2] | **Xueliang Zhang**[1]

[1]Jiangsu Provincial Key Laboratory of Geographic Information Science and Technology, Key Laboratory for Land Satellite Remote Sensing Applications of Ministry of Natural Resources, School of Geography and Ocean Science, Nanjing University, Nanjing, China

[2]Jiangsu Center for Collaborative Innovation in Geographical Information Resource Development and Application, Nanjing, China

Correspondence
Pengfeng Xiao, Jiangsu Center for Collaborative Innovation in Geographical Information Resource Development and Application, 163 Xianlin Avenue, Nanjing 210023, China.
Email: xiaopf@nju.edu.cn

Funding information
National Natural Science Foundation of China, Grant/Award Number: 42171307; Science and Technology Basic Resources Investigation Program of China, Grant/Award Number: 2017FY100502

Abstract

Investigating the spatial and temporal changes in snow cover over mountain areas is significant for understanding the impact of regional climate variability. In this study, using cloud-removed snow cover data, which are generated based on Moderate Resolution Imaging Spectroradiometer (MODIS) daily snow cover products, the spatiotemporal changes of snow cover fraction (SCF) and its relationship with temperature and precipitation changes from 2002 to 2020 were examined over Altai Mountains, China. The results demonstrate that the distribution and changes of SCF are highly spatiotemporally heterogeneous. Within a year, the maximum SCF occurs in January at 98.6%, and the minimum appears in July at 8.7%. The annual-mean SCF shows an increasing trend at 0.09%·annum^{-1}, owing to the significantly increasing SCF in the snow accumulation period at 0.5%·annum^{-1} and the decreasing SCF in the snow melting period at −0.2%·annum^{-1}. The SCF distribution, as well as its inter-annual change, is greatly influenced by elevation. During the snow cover period, a positive linear correlation between SCF and elevation is found at 0.02%·m^{-1} ($p < .01$). The annual-mean SCF decreases in the area below 1,200 m, whereas it increases in the area above 1,200 m. Accordingly, the elevation-dependent SCF results in various SCF distributions on different slopes and watersheds. The SCF shows an apparent pattern in different aspects, with similar SCFs between the north and east aspects and between the west and south aspects but a difference between the northeast aspects and the westsouth aspects. The SCF is negatively correlated with air temperature ($r = -0.74$, $p < 0.01$) and positively correlated with precipitation ($r = 0.74$, $p < 0.01$). In addition, temperature shows a significant and larger correlation with SCF in both the snow accumulation and melting periods, indicating the major factor of temperature for the changes in SCF.

KEYWORDS

Altai Mountains, climate change, MODIS, snow cover change, snow cover fraction

1 | INTRODUCTION

Snow plays an important role in the global energy and water cycle and indicates changes in the global climate and mass movement (Zhang *et al*., 2019a). Snowmelt runoff is an important water source to alleviate spring drought (Dettinger and Cayan, 1995; Ding and Qin, 2009). Mountainous snowmelt provides water to

more than one-sixth of the global population (Barnett *et al*., 2005), with Xinjiang accounting for one-third of China's snowmelt water (Li, 1988). Snowstorms, floods, and other disasters may result from changes in snow accumulation or melting.

In mountain areas, the impact of topography on the snow cover distribution and change should not be overlooked (Beniston, 2012). Previous studies revealed that the altitude of mountain areas influences snow phenology changes. The increased winter temperature results in less snow in the low-to midlatitudes and more snow in high latitudes (McCabe and Wolock, 2010). The length of the snow free season in the middle Tibetan Plateau shortens as the altitude increases (Gao *et al*., 2012). The snow cover fraction (SCF) and snow cover duration (SCD) generally tend to increase with elevation (Tang *et al*., 2017; Marke *et al*., 2018). Slope and aspect also affect snow cover changes (Guo and Li, 2015; Yi *et al*., 2016; Li *et al*., 2019).

There is a strong interaction between snow cover and climate, especially temperature and precipitation, affecting both spatial and temporal snow cover changes (Immerzeel *et al*., 2010; Wang *et al*., 2015; Notarnicola, 2020). Snow cover extent and duration will decrease as a result of global warming (Li *et al*., 2019). A strong negative correlation was found between interannual changes in snow cover and the surface temperature on the Tibetan Plateau (Li *et al*., 2018a; Tang *et al*., 2013), whereas different results of studies on the correlation between snow cover and precipitation are found (Bamzai and Shukla, 1999; Qin *et al*., 2006). In northern Xinjiang of China, a negative correlation between snow cover extent and temperature has been found during accumulation and melt processes (Wang *et al*., 2008). The correlations between snow phenology, temperature, and precipitation vary in different elevation zones in the Central Tianshan Mountains (Wu *et al*., 2019; Wang *et al*., 2021). The variation in temperature and precipitation would lead to changes in the hydrological process, which results in the redistribution of water resources (Li *et al*., 2018b), so the correlation between snow cover and temperature and precipitation needs to be investigated.

Altai Mountains, which connect four countries in Central Asia with a high elevation, are crucial in the global hydrometeorological system. The complex terrain leads to the difference of snow depth on windward slopes and leeward slopes (Zhong *et al*., 2021b), but the impact of slope and aspect on SCF is unknown. Furthermore, Altai Mountains are the areas where snowstorms and snowmelt floods occur frequently (Shen *et al*., 2013). The airstreams of the Arctic Ocean and the Atlantic Ocean provide the majority of the water vapour precipitation in Altai Mountains (Zhang *et al*., 2018), and snowmelt water accounts for 36.9% of the annual runoff in the headwaters of the Irtysh River in Altai Mountains, China (Zhang *et al*., 2017), which can partially cause global climate changes. Research shows that precipitation and temperature show significant upward trends in Altai Mountains, China (Zhang *et al*., 2018), which would affect the hydrological process change in the whole Altai Mountains, and the change trends vary in different regions and seasons. The snow cover duration decreased in the southeastern Altai Mountains, China, based on the sampling collection and analysis of field observation data, while the total snowfall quantity and the maximum snow depth increased (Zhang *et al*., 2017). This means that snow accumulates and melts at a faster rate, as evidenced by other studies (Zhong *et al*., 2021a), which may result in more severe snow disasters. With the development of remote sensing technology, the increasing snow cover duration was found resulting in a decrease in surface temperature in the Altai Mountains, Russia (Van De Kerchove *et al*., 2013). Therefore, more studies on the change and distribution of SCF in the Altai Mountains, China, are needed.

The change in snow cover shows indicative significance to hydrological and meteorological changes. In this study, the Moderate Resolution Imaging Spectroradiometer (MODIS) daily snow cover products are first processed to derive 8-day cloud-removed SCF data; then, the accuracy of the 8-day cloud-removed SCF data is evaluated by comparing the data with the snow cover data extracted from Landsat-8 Operational Land Imager (OLI) images. Subsequently, the spatiotemporal changes in SCF, as well as the effect of elevation on SCF, are studied using 8-day cloud-removed SCF data. Finally, the possible relation between SCF and two main climate parameters, temperature, and precipitation, is explored. The specific aims are to (a) clarify the spatiotemporal changes in snow cover from 2000 to 2020 using remote sensing data, (b) illustrate the influence of terrain (elevation, slope, and aspect) on snow cover patterns and changes, and (c) explore the correlations with temperature and precipitation for snow cover changes supported by meteorological station data.

2 | STUDY AREA

The study area is located in northern Xinjiang Province, China. Altai Mountains, which lie between 85°–90°E and 46°–50°N and stretch from the border of China's northern border to the mainstream of the Irtysh River in the south, are selected (Figure 1). The study area covers an area of 81,300 km^2, with elevations ranging from 409 to 4,312 m. The tributaries of the Irtysh River divide it into four watersheds: Haba River Watershed (HRW), Burqin River Watershed (BRW), Crane River Watershed (CRW), and KalaErzis

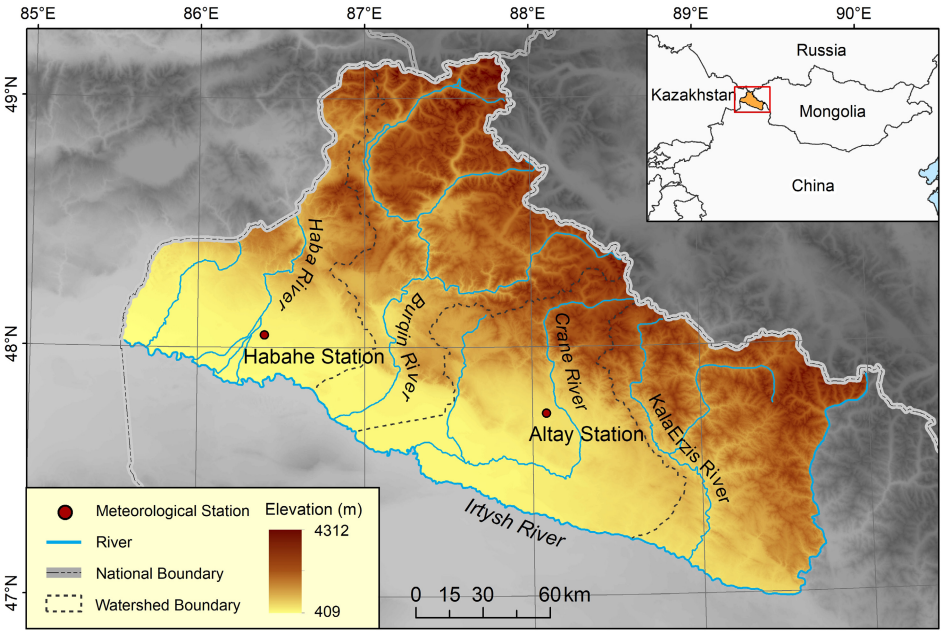

FIGURE 1 Location and extent of the study area [Colour figure can be viewed at wileyonlinelibrary.com]

River Watershed (KRW), which account for 20.8, 30.3, 24.8, and 24.1% of the study area, respectively.

Habahe station (48°3′N, 86°24′E) and Altay station (47°44′N, 88°5′E) are two national meteorological stations in the study area, with altitudes of 533 and 735 m, respectively. The annual-mean temperature and precipitation are 5.3°C and 230 mm, respectively, based on climate data from the two meteorological stations during the study period. The monthly mean temperature reaches a maximum (23°C) in July and a minimum (−15°C) in January. The bimodal distribution of monthly average precipitation presents a maximum in July (25 mm) and November (27 mm) and a minimum in February (11 mm).

3 | DATA

3.1 | MODIS snow cover products

The daily snow cover products MOD10A1(V006) (from Terra) and MYD10A1 (from Aqua) (Hall *et al.*, 2016) derived from MODIS are employed to investigate the spatio-temporal changes in SCF. The study period from September 1, 2002 (the beginning of the first snow year) to August 31, 2020 (a total of 18 years) was selected since Aqua was successfully launched on May 4, 2002. The spatial resolution is 500 m. The two MODIS snow cover products are derived by SNOMAP (Hall *et al.*, 1995), a snow mapping algorithm based on Normalized Difference Snow Index (NDSI). The quality band "NDSI_Snow_Cover_Basic_QA" in this product is used for quality control of MODIS snow cover products.

The NDSI identifies snow based on the spectral differences of the reflectance between snow and clouds in the visible and shortwave infrared bands. The SNOMAP algorithm sets the threshold of NDSI and eliminates the influence of water and forest cover on snow detection (Chen *et al.*, 2010; Jiang and Wang, 2017). The algorithm is as follows:

$$\mathrm{NDSI}=\frac{r_4-r_6}{r_4+r_6}, \tag{1}$$

where r_4 is the reflectance in MODIS band 4 (0.545–0.565 μm) and r_6 is that in band 6 (1.628–1.652 μm). The conditions for detecting snow are as follows:

$$(\mathrm{NDSI}\geq 0.4)\cap(r_2>0.1)\cap(r_4>0.1), \tag{2}$$

where r_2 is the reflectance of MODIS band 2 (0.841–0.876 μm).

The SNOMAP algorithm improves snow detection, but weather conditions still have an impact on the accuracy of snow cover products (Hall and Riggs, 2007). In northern Xinjiang Province, the mean accuracy of snow cover identification in MODIS daily snow cover products is 33.7%, but it is 87.3% in MODIS 8-day composite snow cover products (Huang *et al.*, 2007).

3.2 | Landsat-8 OLI images

The Landsat-8 OLI images are used to evaluate the accuracy of the MODIS 8-day cloud-removed snow cover products. The images are provided by the United States

Geological Survey (USGS) with a revisit interval of 16 days and underwent atmospheric correction and topographic correction. Each image contains seven bands, including visible, near infrared, and shortwave infrared bands, with a spatial resolution of 30 m. The study area is covered by seven tiles of Landsat-8 OLI images, including h145v26, h144v26, h143v26, h145v27, h144v27, h143v27, and h142v27. During the study period, 157 days of images are selected.

3.3 | Elevation data

Digital Elevation Model (DEM) data are used to examine the influence of elevation on SCF change. The DEM data are derived from the Shuttle Radar Topography Mission (SRTM) data from the Jet Propulsion Laboratory (JPL) (Farr *et al.*, 2007). Based on elevation data, the SRTM provides a high-resolution digital topography database with spatial resolutions of 30 m, 90 m, and 1 km. Elevation data with a 30-m resolution are used in this study (see Figure 1). Based on the physical regionalization and the area proportion of different elevation zones, the elevation data are reclassified into four elevation zones: <1,200 m (zone A), 1,200–2,300 m (zone B), 2,300–3,000 m (zone C), and >3,000 m (zone D). The proportions of the four watersheds and the study area belonging to different elevations are shown in Table 1.

The slope and aspect are calculated using the elevation data. The study area is divided into three slope zones and four aspect zones based on the distribution characteristics of the slope and aspect. The area proportions of the slope zones and aspect zones in the study area are shown in Table 2. The slope zones are derived from the combination of adjacent zones with similar annual and interannual change trends of SCF, with the area with a slope greater than 15° accounting for a relatively small proportion of the total. The south and west slopes are approximate twice the proportion of the north and east slopes in terms of area.

3.4 | Meteorological data

The temperature and precipitation data from the Habahe and Altay meteorological stations are used as the meteorological data. The monthly mean temperature and precipitation data of the meteorological stations are collected from the National Meteorological Information Center (http://data.cma.cn). Due to the similarity of the geographical environments of the two meteorological stations, the mean temperature and precipitation data of the two meteorological stations are used to represent those of the study area.

4 | METHOD

4.1 | Combining 8-day cloud-removed snow cover product

The cloud obscuration of MODIS daily snow cover products must be removed to make the calculated snow cover fraction closer to the surface condition under clouds (Xie *et al.*, 2009; Paudel and Andersen, 2011; Li *et al.*, 2017). The mean cloud cover percentage of the study area is 47.9% for the Terra product and 49.2% for the Aqua product. Based on the difference in transit time between the Terra and Aqua platforms, which is 1030 LST in Terra and 0130 LST in Aqua, the cloud coverage could be decreased by combining MOD10A1 and MYD10A1. The influence of clouds in single-day data can be further

TABLE 1 Area proportions (%) of the four watersheds and the study area in the four elevation zones

Elevation zone	HRW	BRW	CRW	KRW	Study area
A	67.43	19.76	68.04	22.49	42.35
B	27.39	43.35	22.01	51.00	36.48
C	5.07	33.03	9.73	24.50	19.36
D	0.11	3.86	0.22	2.01	1.81

TABLE 2 Area proportions (%) of the three slope zones and the four aspect zones in the study area

	Slope zone			Aspect zone			
Zone	<5°	5–15°	>15°	North (315°–360° and 0°–45°)	East (45°–135°)	South (135°–225°)	West (225°–315°)
Area proportion	45.36	35.61	19.03	16.32	19.02	34.44	30.22

removed by combining the data on multiple dates (Dietz *et al.*, 2012).

Therefore, an 8-day combining method is proposed to obtain the MODIS cloud-removed snow cover product. The cloud removal process is implemented in three steps. First, the quality flag band "NDSI_Snow_Cover_Basic_QA" is used to select the pixels with high confidence in the MODIS snow cover products. Selecting the pixels with a value of 0 or 1 in the quality flag band represents that the pixels are of best or good quality. Then, the pixels corresponding to it in MODIS snow cover products are extracted as the pixels with high confidence. Second, all images in MOD10A1 and MYD10A1 are divided into two types of pixels: snow and nonsnow. Third, the images are combined every 8 days using the following prioritization scheme: snow has priority, which means that if a pixel in any input image is snow, the pixel will be snow in the combined image at the same position. Finally, the cloud-removed snow cover product from 2002 to 2020 was generated, which includes 776 images.

4.2 | Generating reference data for accuracy assessment

The reference data are generated based on Landsat-8 OLI snow cover data using the snow-mapping algorithm SNOMAP (Hall *et al.*, 1995) from Landsat-8 OLI images. The equation is shown as follows:

$$\mathrm{NDSI}=\frac{r_3-r_6}{r_3+r_6}, \tag{3}$$

where r_3 is the reflectance in Landsat-8 OLI band 3 (0.53–0.59 μm) and r_6 is that in band 6 (1.57–1.65 μm). The condition for detecting snow is as follows:

$$(\mathrm{NDSI}\geq 0.4)\cap(r_5>0.1)\cap(r_3>0.1), \tag{4}$$

where r_5 is the reflectance in Landsat-8 OLI band 5 (0.85–0.88 μm). The spatial resolution of the Landsat-8 OLI snow cover data is resampled from 30 to 500 m, with pixels labelled as snow when more than half of them are covered by snow (Hall *et al.*, 2002).

It is noted that the snow observation data of the meteorological stations are not used for assessing accuracy. The possible biases caused by elevation, slope, and aspect may be overlooked when using these data to assess accuracy because of the difference in scales and the uneven distribution of meteorological stations. The use of Landsat-8 OLI snow cover data can compensate for the uncertainty in accuracy assessment (Salomonson and Appel, 2004; Huang *et al.*, 2011).

4.3 | Accuracy assessment of the cloud-removed snow cover product

The generated reference data are used to assess the accuracies of the cloud-removed snow cover products in different elevation zones. The confusion matrix is used to calculate the overall accuracy (OA), precision (P), and recall (R). OA indicates the fraction of correctly classified pixels among all pixels, P indicates the fraction of correctly classified snow pixels among the classified snow pixels, and R is the fraction of snow pixels that are classified. The formulas are as follows:

$$\mathrm{OA}=\frac{\mathrm{TP}+\mathrm{TN}}{\mathrm{TP}+\mathrm{FN}+\mathrm{FP}+\mathrm{TN}}, \tag{5}$$

$$P=\frac{\mathrm{TP}}{\mathrm{TP}+\mathrm{FP}}, \tag{6}$$

$$R=\frac{\mathrm{TP}}{\mathrm{TP}+\mathrm{FN}}, \tag{7}$$

where TP is the count of snow pixels that are classified as snow, TN is that of nonsnow pixels that are classified as nonsnow, FP is that of nonsnow pixels that are classified as snow, and FN is that of snow pixels that are classified as nonsnow.

4.4 | Methodology of snow cover changes

The SCF and proportion of snow cover days (PSCD) from cloud-removed snow cover product are used to present the spatiotemporal distribution and changes in snow cover. The SCF in a given region is expressed as

$$\mathrm{SCF}=\left(\frac{N_s}{N_a}\right)\times 100\%, \tag{8}$$

where N_s is the number of snow cover pixels and N_a is the number of all pixels.

The monthly mean and annual-mean SCF are derived to investigate the snow cover changes at different time scales. Because the temporal resolution of the cloud-removed snow cover product is 8 days, the monthly mean SCF is calculated as

$$\mathrm{SCF}_m=\frac{\sum_{y=1}^{18}\sum_{i=1}^{n_{ym}}\mathrm{SCF}_{ymi}}{n_{ym}\times 18}, \tag{9}$$

where SCF_m is the monthly mean SCF in month m; SCF_{ymi} is the SCF of image i in month m in year y; n_{ym} is

the number of images in month m in year y; and 18 means that a total of 18 years of snow cover data are used.

The annual-mean SCF is derived as

$$\mathrm{SCF}_y = \frac{\sum_{i=1}^{n_y} \mathrm{SCF}_{yi}}{n_y}, \tag{10}$$

where SCF_y is the annual-mean snow cover data of year y; SCF_{yi} is the SCF of image i in year y; and n_y is the number of images in year y.

The proportion of snow cover days (PSCD) in a pixel is the proportion of the snow cover days to the total days. The PSCD during a given period is calculated as

$$\mathrm{PSCD} = \left(\frac{D_s}{D_t}\right) \times 100\%, \tag{11}$$

where D_s is the number of snow days and D_t is the number of total days.

Linear regression analysis methods are used to simulate the change trend of a time series. The least square regression method is employed to calculate the change trends of SCF under different spatiotemporal conditions. The slope (s) of the least squares line fitting of SCF is expressed as

$$s = \frac{n\sum_{i=1}^{n} x_i y_i - \sum_{i=1}^{n} x_i \sum_{i=1}^{n} y_i}{n\sum_{i=1}^{n} x_i{}^2 - \left(\sum_{i=1}^{n} x_i\right)^2}, \tag{12}$$

where s is the slope of the least square line fitting; x_i is the series number for the years from 2002 to 2020 or the elevation divisions; n is the cumulative number of years or elevation divisions; and y_i is the value of SCF in the year or in the elevation division x_i.

4.5 | Linkage between snow cover and precipitation and temperature

Pearson correlation analysis is used to evaluate the linear correlation between SCF and temperature and precipitation. Pearson correlation coefficient (r) is expressed as

$$r_{xs} = \frac{\sum_{i=1}^{n} (x_i - \overline{x})(s_i - \overline{s})}{\sqrt{\sum_{i=1}^{n} (x_i - \overline{x})^2} \sqrt{\sum_{i=1}^{n} (s_i - \overline{s})^2}}, \tag{13}$$

where r_{xs} is the correlation coefficient between x and s; x denotes the value of the climate factor; s denotes the SCF; $\overline{x}$ and $\overline{s}$ are the mean values of x and s, respectively; and n is the number of samples.

The significance levels (p) of the analyses in change trends and correlation are presented, in which the correlation is considered significant if it is at the 5 or 1% confidence level.

5 | RESULTS

5.1 | Accuracy of the cloud-removed snow cover product

The cloud-removed snow cover product is evaluated by comparing the cloud cover fraction before and after cloud removal, as shown in Figure 2. The cloud cover fraction before cloud removal is represented by the mean value of that in MOD10A1 and MYD10A1 on the same date. The cloud cover fraction decreases during most of the study period. The mean cloud cover fraction decreases from 48.2 to 20.4%, and it decreases obviously from 50.5 to 15.3% during the period from September to May of the next year. The mean cloud cover fraction decreases slightly by 8.8 percentage units from June to August. This result suggests that it is effective to reduce the cloud cover fraction from snow cover data, especially during the snow season.

A confusion matrix is used to assess the accuracy of the cloud-removed snow cover data in different elevation zones and periods, and the one from September to May of the next year is shown in Table 3. The P and R in the whole study area are 72.0 and 95.0%, respectively, from September to May of the next year. With increasing elevation, P and R show downward trends with a peak in zone B and upward trends with a valley in zone C, respectively. The OA reaches the maximum (88.6%) and minimum (70.0%) in zones A and B, respectively. The accuracy assessment shows that the cloud-removed snow cover product is reliable for monitoring SCF changes in the study area.

5.2 | Temporal change of snow cover fraction

The annual cycle of SCF shows strong seasonal change as shown in Figure 3a. The mean SCF over the study area is approximately 52%. The highest SCF occurs in January, reaching 98.6%, while the lowest appears in July, at approximately 8.7%. From the middle of September to the end of May, the SCF is greater than 20%. Relatively large interannual deviations are found in this period except in December–February when the study area is

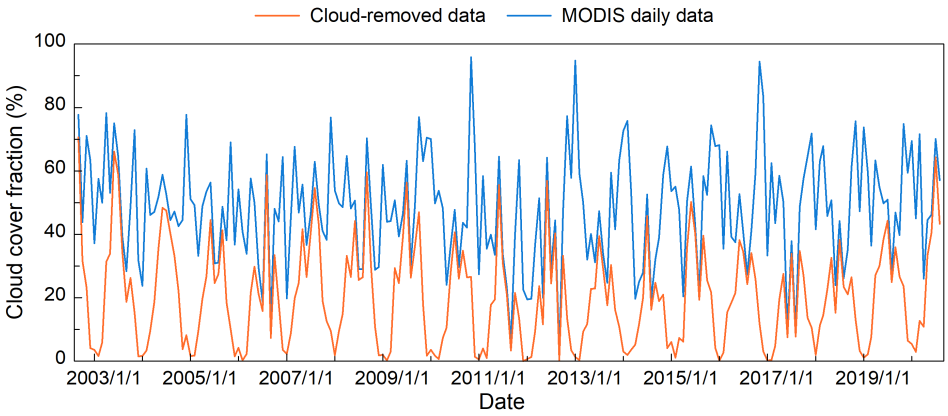

FIGURE 2 Cloud cover fraction of the snow cover data before and after cloud removal from 2002 to 2020 [Colour figure can be viewed at wileyonlinelibrary.com]

TABLE 3 Accuracy of the cloud-removed snow cover product in the four elevation zones during September–May of the next year from 2002 to 2020

Elevation zone	*P* (%)	*R* (%)	OA (%)
A	79.7	92.7	88.6
B	60.1	95.7	70.0
C	77.8	99.1	79.2
D	74.1	97.8	74.5
Overall	72.0	95.0	79.0

nearly completely covered by snow. The SCF is approximately 10% in June and subsequently decreases to below 10% in July and August, with a small interannual change.

Figure 3b shows the interannual change in SCF in the five subperiods, and the linear trends (slope, %·annum^{-1}) of that in each month are presented in Table 4. Five subperiods are divided based on the abovementioned seasonal change, including the snow accumulation period (SAP, from September to November), snow stable period (SSP, from December to February), snow melting period (SMP, from March to May), snow free period (SFP, from June to August), and snow cover period (SCP, from September to May of the next year). The interannual fluctuation of SCF in SCP is between 59 and 72% and shows upward trends at 0.09%·annum^{-1}. In SAP and SMP, the fluctuations in the annual-mean SCF show large interannual changes, whereas those in SSP and SFP are lower. In SAP, the SCF increases with snow accumulation, and the spread of the annual-mean SCF is between 32 and 52%, with a significant upward interannual trend of 0.5%·annum^{-1}. Increases also occur in all months of SAP, especially in September and October, with significant increases at 0.47 and 0.87%·annum^{-1}, respectively. The spread of SMP is between 45 and 74% with an abnormally high value in 2010. This may be caused by the abnormal snowstorms in January of that year, which make the snow amount at the beginning of the year larger than in other years. A downward trend of SCF is found in SMP at −0.2%·annum^{-1}. Accelerated snow accumulation in SAP has a greater influence on the increase in SCF during SCP than accelerated snow melting during SMP. This would impact both agricultural irrigation and industrial production. The risk of flood disasters increases in SMP, and the acceleration of snow accumulation leads to snow disasters in SAP.

5.3 | Spatial distribution of snow cover fraction

The annual cycle and interannual change in SCF in the four elevation zones are analysed to investigate the distribution and change trend of SCF at different elevation zones (Figure 4). The peak annual SCF is close to 100% for all elevation zones in SSP, whereas the differences in SCF between the four elevation zones are mainly reflected in the snow accumulation and melting processes. With increasing elevation, the onset of snow melt tends to delay, and snow accumulation begins earlier. In zone A, snow starts to accumulate in late September, reaches a peak (97%) in January, and then rapidly drops to less than 1% from May to August. In zone B, the SCF is highest in mid-November and remains steady until mid-March, and then the snow melts to approximately 10% in mid-June to mid-September. The highest SCF in zone C remains for 7 months (during mid-October and mid-May), with the lowest SCF of 18%. In zone D, the SCF remains the highest value from October to May, and the lowest value occurs in July at approximately 60%, which is far higher than that in the other three elevation zones.

SCF shows opposite interannual change trends above and below 1,200 m. With the highest range of fluctuation in the four elevation zones, the SCF in zone A shows a weakly downward trend at −0.08%·annum^{-1}. With increasing elevation, the interannual fluctuation in SCF

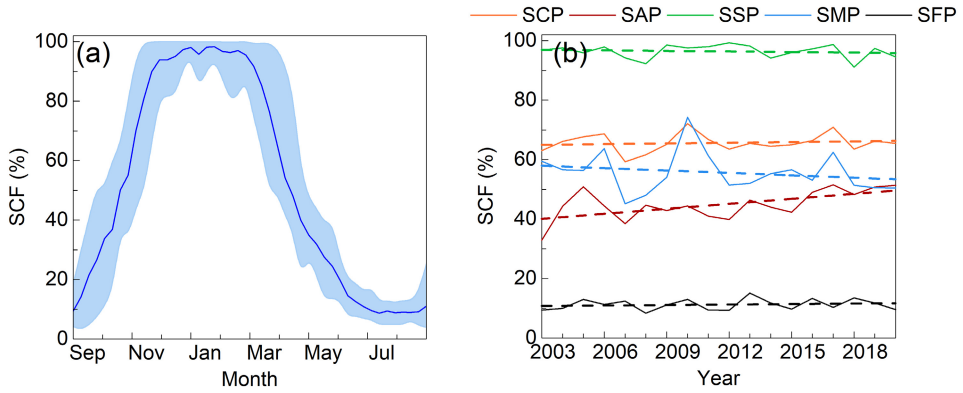

FIGURE 3 Annual cycle of SCF (a) and interannual change in SCF (b) during the snow cover period (SCP), snow accumulation period (SAP), snow stable period (SSP), snow melting period (SMP), and snow free period (SFP) over the study area from 2002 to 2020. The error bars in (a) show the standard deviation, indicating the interannual changes [Colour figure can be viewed at wileyonlinelibrary.com]

TABLE 4 Interannual linear trends (slope, %·annum^{-1}) of monthly mean SCF from 2002 to 2020

Period	SCP	Sep	Oct	Nov	Dec	Jan	Feb	Mar	Apr	May	Jun	Jul	Aug
Slope	0.09	0.97*	0.60*	0.11	−0.16	0.01	−0.04	−0.25	−0.46	−0.10	0.19	0.06	−0.08

Note: *Statistical significance at the 0.05 level.

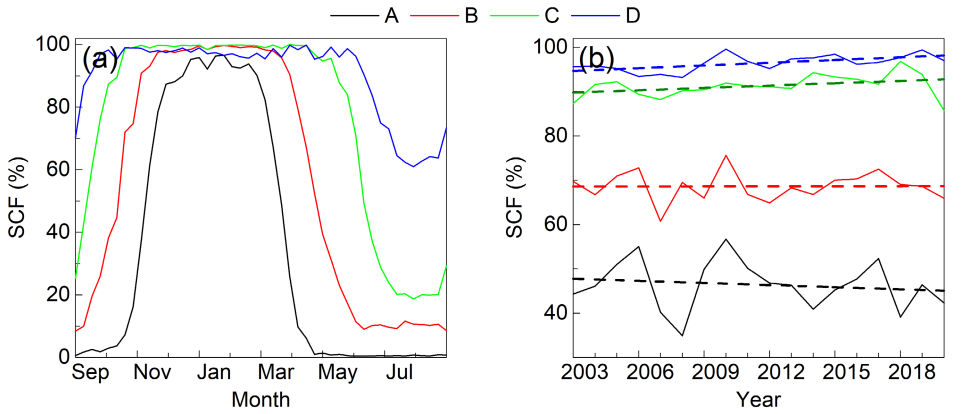

FIGURE 4 Annual cycle change in SCF (a) and interannual change in SCF during the snow cover period (b) in the four elevation zones over the study area from 2002 to 2020 [Colour figure can be viewed at wileyonlinelibrary.com]

decreases. The SCF increases in zone B at 0.14%·annum^{-1}. In zones C and D, the SCF increases significantly at 0.31 and 0.14%·annum^{-1}, respectively.

The annual-mean SCF is higher at high elevations than at low elevations. To show the elevation-related SCF distribution, the mean, maximum, and minimum SCF per 50 m in SCP are calculated (Figure 5). The significantly positive correlation between SCF and elevation is confirmed with an equal increase of 0.02%·m^{-1}. In zones A, B, and C, the mean SCF increases significantly at 0.02, 0.03, and 0.01%·m^{-1}, respectively, with no significant correlation with the elevation in zone D. The maximum and minimum SCFs are positively correlated with elevation. The maximum SCF increases at 0.03%·m^{-1} below 800 m and approaches its maximum above 800 m. The minimum SCF has little correlation with elevation below 1,000 m but increases significantly at 0.04%·m^{-1} above 1,000 m.

The spatial distribution and the annual change trends of the annual mean PSCD also show obvious spatial

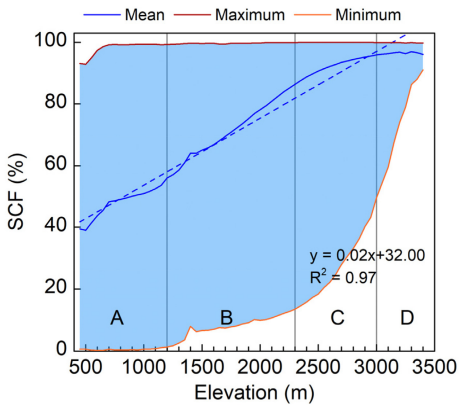

FIGURE 5 Mean, maximum, and minimum SCF at different elevations during the snow cover period over the study area from 2002 to 2020 [Colour figure can be viewed at wileyonlinelibrary.com]

heterogeneity (Figure 6). PSCD is lower in the south and higher in the north, and it increases with increasing elevation. The PSCD is less than 30% in the southwestern

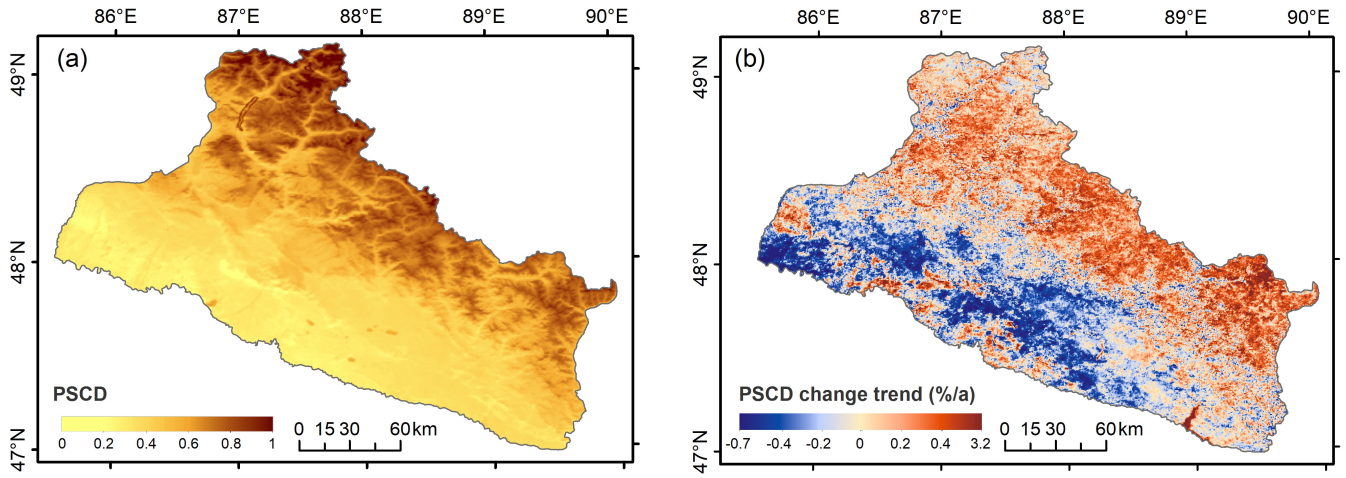

FIGURE 6 Spatial distribution of PSCD (a) and its change trend (b) during the snow cover period over the study area from 2002 to 2020 [Colour figure can be viewed at wileyonlinelibrary.com]

FIGURE 7 Annual cycle change in SCF (left column) and interannual change in SCF during the snow cover period (right column) in the three slope zones (a, b) and the four aspect zones (c, d) over the study area from 2002 to 2020 [Colour figure can be viewed at wileyonlinelibrary.com]

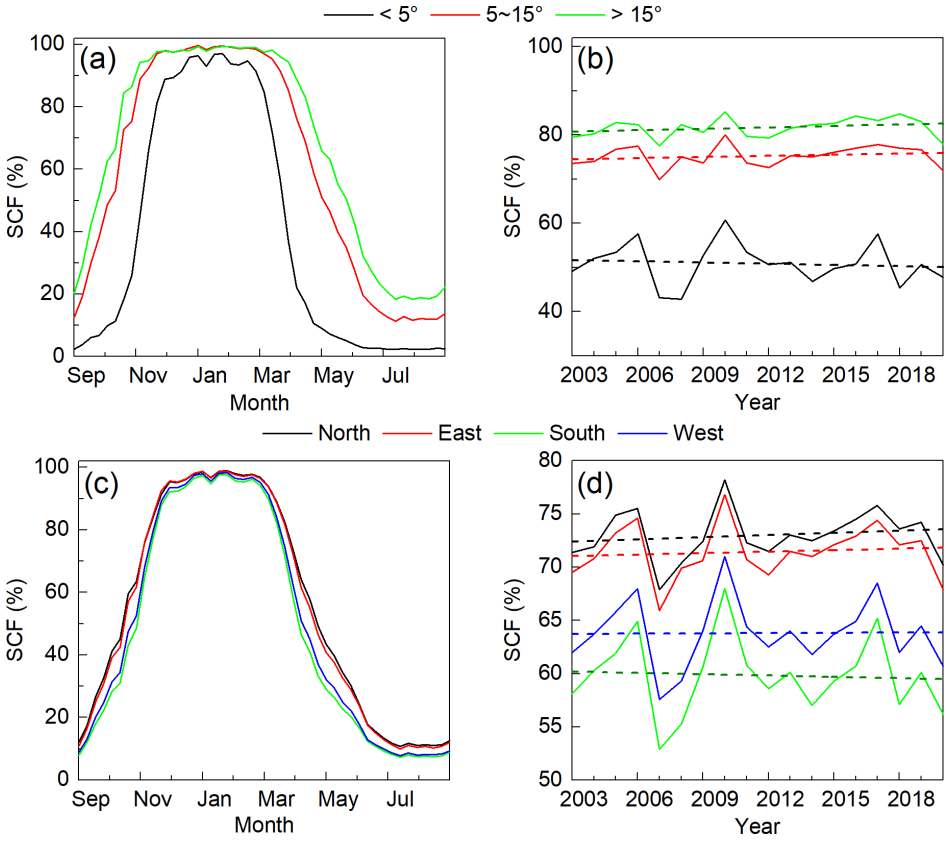

part of the study area, lower elevation. The high-value area of PSCD is mainly distributed in the north, with 100% in the northwest. The change trend of PSCD decreases in the southwest and increases in the northeast. The area where PSCD decreases is at a lower elevation with a lower PSCD, while the area where PSCD increases is mostly the area with a higher PSCD and elevation. These trends indicate that the difference of PSCD between high and low elevation areas increases, and its spatial heterogeneity would be more obvious. The value and change trends on SCF and PSCD show similar characteristics. The analysis on PSCD could enrich the understanding of the spatial distribution characteristics of SCF.

A higher SCF appears in the zones with steeper slopes (Figure 7a). In addition, the SCF reaches a peak earlier and starts to decline later in the steeper slope zone. As shown in Figure 7b, the interannual change in SCF in the slope zone below 5° has a slightly decreasing trend at

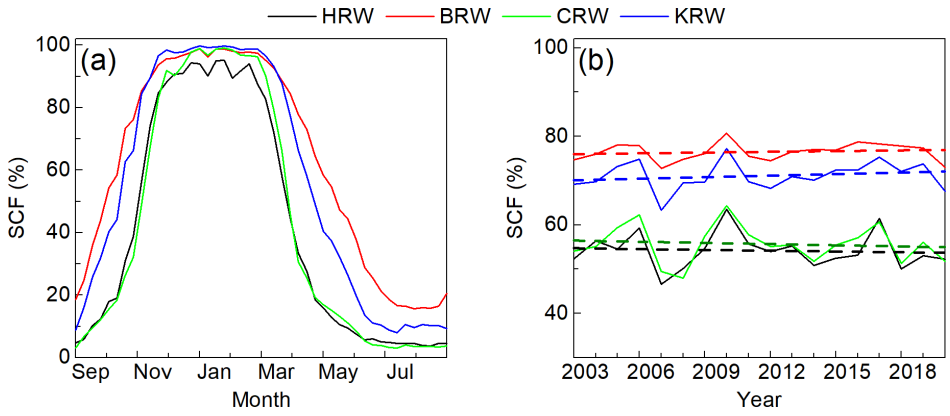

FIGURE 8 Annual cycle change of SCF (a) and interannual change in SCF during the snow cover period (b) over the four watersheds from 2002 to 2020 [Colour figure can be viewed at wileyonlinelibrary.com]

$-0.04\%\cdot\text{annum}^{-1}$, which is opposite to the two slope zones above 5°. The SCF increases in the slope zone between 5° and 15° at $0.17\%\cdot\text{annum}^{-1}$, whereas it increases significantly at $0.21\%\cdot\text{annum}^{-1}$ in the slope zone above 15°. SCF changes could be closely related to elevation because the slope tends to be large in high elevation areas.

The SCF shows a descending order from the northern, eastern, western, to southern aspects in Figure 7c,d. The change trends of both annual and interannual fluctuations in SCF are similar in the northern and eastern zones, as well as in the southern and western slopes. However, the SCF changes are different between the northeast zone and southwest zone. The mean difference of SCF between the north and east slopes is 0.8% and that between the south and west slopes is approximately 1.7%. However, the mean SCF difference between the northeast slope and southwest slope reaches 5.7%. The interannual SCFs in the northern, eastern, and western aspects show increasing trends at 0.07, 0.05, and $0.01\%\cdot\text{annum}^{-1}$, respectively. In contrast, the interannual SCF in the southern aspect shows a decreasing trend at $-0.04\%\cdot\text{annum}^{-1}$.

5.4 | Change of snow cover fraction in watersheds

The change trends of SCF in BRW and KRW are similar due to their close proportion in each elevation zone, and those in HRW and CRW are also similar for this reason (Figure 8). From the middle of November–February, the SCF of each watershed remains at its peak, with peaks at approximately 96% in HRW and over 99% in other watersheds. In other periods within a year, the SCF of BRW is the highest, followed by KRW, and the SCF of HRW and CRW is the lowest with a difference of less than 3%. The largest difference in SCFs among the four watersheds occurs between BRW and CRW in April and October, that is, in the middle of SAP and SMP, reaching approximately 47%. The annual-mean SCFs in BRW (approximately 72–80%) and KRW (approximately 63–77%) increase at 0.14 and $0.21\%\cdot\text{annum}^{-1}$, respectively. The fluctuations of the annual-mean SCF in HRW and CRW are approximately 46–64%, with slight downward trends at −0.03 and $-0.02\%\cdot\text{annum}^{-1}$, respectively.

5.5 | Response of snow cover fraction to climate factors

SCFs show correlations with temperature and precipitation in terms of both annual and interannual changes (Figure 9). The monthly SCF trend is inverse to the temperature trend within a year. The monthly mean precipitation peaks in November and July, showing a lagged effect on SCF. The annual-mean temperature and precipitation increase at $0.02°\text{C}\cdot\text{annum}^{-1}$ and $0.14\ \text{mm}\cdot\text{annum}^{-1}$, respectively, which are consistent with the trend of SCF.

Tables 5 and 6 present the Pearson correlation coefficients between the SCF and temperature and precipitation at both monthly and annual scales, respectively. The SCF is mostly negatively correlated with temperature and positively correlated with precipitation in different months (Table 6). In SCP, the temperature has a slightly higher correlation coefficient than precipitation, indicating a greater impact on SCF change. The changes in temperature and precipitation have little effect on the change in SCF after it reaches its peak in SSP, leading to insignificant correlations between SCF and temperature and precipitation. The correlations between temperature and SCF in SAP and SMP are significantly negative and higher than those between precipitation and SCF, suggesting that temperature changes during the two periods would accelerate or retard snow accumulation and melting. Since the

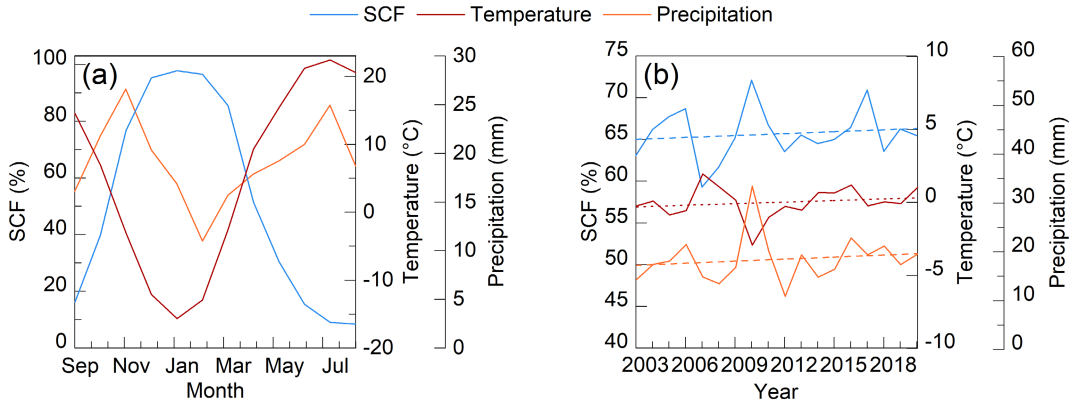

FIGURE 9 Monthly mean (a) and annual-mean (b) SCF, temperature, and precipitation over the study area from 2002 to 2020 [Colour figure can be viewed at wileyonlinelibrary.com]

TABLE 5 Pearson correlation coefficients between the monthly mean SCF and temperature and precipitation from 2002 to 2020

Month	Temperature	Precipitation
September	−0.64*	0.66*
October	−0.54**	0.37
November	−0.74*	0.46
December	−0.54**	0.18
January	−0.37	−0.52**
February	−0.37	0.52**
March	−0.84*	0.11
April	−0.78*	0.01
May	−0.50**	0.33
June	−0.16	0.35
July	−0.15	−0.05
August	−0.29	0.06

Note: * and ** indicate statistical significance at the 0.01 and 0.05 levels, respectively.

TABLE 6 Pearson correlation coefficients between the annual-mean SCF and temperature and precipitation of different periods

Period	Temperature	Precipitation
SAP	−0.39	0.57**
SSP	−0.24	0.42
SMP	−0.54**	0.31
SFP	−0.27	0.31
SCP	−0.74*	0.74*

Note: * and ** indicate statistical significance at the 0.01 and 0.05 levels, respectively.

interannual change in SCF is mainly caused by the SCF in SAP and SMP, temperature could play a major role in the SCF change.

6 | DISCUSSION

6.1 | Impact of terrain on snow cover fraction

We already know that there is significant spatiotemporal heterogeneity in the distribution of snow cover over the study area. The fluctuation trends of SCF at different elevations and subregions are similar to the overall trend in the study area, but their extreme values and starting and ending dates in various snow cover periods are different. The percentage of different slope zones and aspect zones in each elevation zone is calculated to explore the physical mechanisms that influence the distribution of snow cover, as shown in Table 7.

The higher the elevation in the four elevation zones, the higher its annual minimum and interannual-mean SCF, showing a correlation between the overall SCF and elevation in the study area (Figure 4). As shown in Figure 7a,b, the SCF of different slope zones increases with increasing slope. Correspondingly, the percentage of slope zones in higher elevation zones shows a similar pattern. In this case, the SCF in slope zones correlates with its elevation percentage.

The differences in the annual-mean SCF in different aspect zones are small, as shown in Figure 7c, which corresponds to the smaller differences in their percentages in the higher elevation zones. In the SAP and SMP, the differences between northeast and southwest aspects are larger than in other periods of the year, which may be because snow cover accumulates (melts) faster (slower) in the higher elevation zones than in the lower elevation zones, and also that northeast aspects have a higher share in higher elevation zones than southwest aspects.

Among the interannual changes in SCF in different zones, the SCF in 2010 shows anomalously high values. As shown in Figure 9b, the phenomenon is caused by

TABLE 7 Area proportions (%) of the three slope zones and the four aspect zones in the four elevation zones

Elevation zone	Slope zone			Aspect zone			
	<5°	5°–15°	>15°	North	East	South	West
A	72.69	7.53	1.35	15.67	16.03	34.24	26.94
B	16.44	33.46	22.30	28.01	27.40	23.22	23.47
C	6.56	33.59	31.75	30.28	29.89	20.95	22.80
D	4.31	25.42	44.60	26.04	26.67	21.59	26.79

elevated precipitation, which in turn is due to the combined effect of the westerly blowing action and the greater precipitation in the western part of the study area in 2010 than in the previous 2 years (Yi *et al.*, 2016), which is consistent with the conclusions on the correlation between SCF and precipitation in this study.

6.2 | Comparison with previous studies

The results obtained in the study are compared with those of previous studies, and the potential reasons for their consistency and inconsistency are discussed. The maximum and minimum SCFs in the Altai Mountains, according to our research, occur in the winter and spring, respectively. Several studies have shown that the highest and lowest SCFs in the Tianshan Mountains occur in January–February and August, respectively (Tang *et al.*, 2017), while the two maximum and relative minimum SCFs in the Tibetan Plateau occur in spring and autumn and winter (Tang *et al.*, 2013; Li *et al.*, 2018a; Zhong *et al.*, 2021a). This illustrates the regional differences in climate and topography between the Altai Mountains and the Tibetan Plateau. Despite their large latitudinal differences, there are parallels between the Tianshan Mountains and the Altai Mountains, which are both mountain areas.

A previous study showed a decrease in snow cover duration at the meteorological station on the KalaErzis River (Zhang *et al.*, 2017), whereas the SCF in the lower elevation zone of the KalaErzis River showed a slightly increasing trend in our study. The difference between the two results may be explained by the scale difference between the data used in the two studies. The results obtained from the analysis of meteorological station data would be more consistent with the ground conditions of the meteorological station but less applicable than those obtained using remote sensing data, making it difficult to comprehensively analyse the distribution and change in SCF.

Another study found that in Altai Mountains, leeward slopes are more likely to accumulate snow, especially on north-, east-, and southeast-facing slopes (Zhong *et al.*, 2021b), which helps to explain the distribution of SCF in different aspect zones in our study. It was found that impurities such as soot and dust aerosols indirectly lead to the accelerated reduction of snow cover over the western China mountains (Li *et al.*, 2021), and this phenomenon has also been found in the eastern part of Altai Mountains, China (Zhang *et al.*, 2019a; Zhong *et al.*, 2021a), but more data are needed to analyse the effect on the whole study area.

The negative correlation between temperature and SCF is consistent with the findings in other areas (Tang *et al.*, 2013; Li *et al.*, 2018a; Schöner *et al.*, 2019); however, both temperature and SCF in the Altai Mountains show increasing trends from year to year over the study period. The studies show that the effect of temperature change on SCF depends on the correlation between winter temperature and precipitation. When the winter temperature is well below freezing, the change trend of SCF is more influenced by precipitation than by temperature (Ye and Mather, 1997; Qin *et al.*, 2006).

6.3 | Limitations and further study

The snow recognition accuracy of the daily snow cover products MOD10A1 and MYD10A1 may be affected by many factors, such as complex terrain and cloud cover. In the area except for zone B, the P of the cloud-removed snow cover product decreases as the elevation increases, while R increases. Since the cloud-removal method is based on snow cover information, the cloud-removal effect is not obvious in SFP, and there is still a small amount of cloud cover in the cloud-removed snow cover product. Remote sensing data with less cloud cover and at finer spatial resolution can be used in further studies to analyse the snow cover in the study area.

Two meteorological stations could be found in the study area, and it was discussed whether the spatial representation of the stations was appropriate to represent the study area. We calculated the correlations between SCF and meteorological data at different elevations, and the results show that those correlations are significant in the study area. A study also showed that the Altay station

is somewhat spatially representative (Wang *et al*., 2011). Moreover, the site data have higher accuracy than reanalysis data (Hu *et al*., 2019; Zhang *et al*., 2019b), which show significant underestimation in northern Xinjiang (Shan *et al*., 2020). Additionally, the spatial resolutions of the reanalysis data are coarser than those of the snow cover products used in this study (Wu *et al*., 2016). Therefore, meteorological station data are selected to analyse the correlation between SCF and meteorological data in this study. More data on temperature and precipitation at the higher elevation zones in the study area will be collected in further studies, either by collection or measurement.

7 | CONCLUSION

In this study, the spatiotemporal characteristics and change trends of SCF in Altai Mountains, China, from September 1, 2002, to August 31, 2020, are analysed based on the MODIS snow cover product, and the relationships between SCF and temperature and precipitation are also investigated. The distribution of SCF exhibits large spatiotemporal heterogeneity over the study area. The maximum (98.6%) and minimum (8.7%) SCFs occur in January and July, respectively. The mean SCF in the snow cover period shows an increasing trend at 0.09%·annum^{-1}. However, the SCFs in SAP and SMP show increasing (0.5%·annum^{-1} significantly) and decreasing (−0.2%·annum^{-1}) trends, respectively. This shows that the interannual increasing trend of SCF over the study area is closely related to the speed of snow accumulation or melting.

A significant positive linear correlation between SCF and elevation in SCP is found at 0.02%·m^{-1}. The SCF decreases in zone A at −0.08%·annum^{-1} but increases in zones B, C, and D at 0.14, 0.31%·annum^{-1} significantly, and 0.14%·annum^{-1} significantly, respectively. The influence of slopes on SCF is based on elevations. The SCF shows a similar pattern and change between the north and east aspects as well as between the west and south aspects but an apparent difference between the northeast and southwest aspects. Furthermore, the order of the mean SCF over watersheds is consistent with the proportion of watersheds in the area above 1,200 m, indicating that elevation is the dominant factor that affects the distribution of SCF over the study area.

The SCF over the study area shows a significant negative correlation with temperature ($r = -0.74$) and a significant positive correlation with precipitation ($r = 0.74$). In SAP and SMP, the temperature is the major factor influencing the changes in the annual-mean SCF. The change trends of the two climate factors in these periods will affect the processing of snow accumulation and snow melting in the study area and may increase the occurrence of snow disasters or decrease the occurrence of snowmelt floods.

ACKNOWLEDGEMENTS

This work was supported in part by the National Natural Science Foundation of China under Grant 42171307 and in part by the Science and Technology Basic Resources Investigation Program of China under Grant 2017FY100502.

AUTHOR CONTRIBUTIONS

Shen Qin: Data curation; formal analysis; methodology; validation; visualization; writing – original draft; writing – review and editing. **Pengfeng Xiao:** Conceptualization; data curation; formal analysis; methodology; validation; visualization; writing – original draft; writing – review and editing. **Xueliang Zhang:** Conceptualization; supervision; writing – original draft; writing – review and editing.

ORCID

Shen Qin https://orcid.org/0000-0002-0701-1082
Xueliang Zhang https://orcid.org/0000-0001-6188-0257

REFERENCES

Bamzai, A.S. and Shukla, J. (1999) Relation between Eurasian snow cover, snow depth, and the Indian summer monsoon: an observational study. *Journal of Climate*, 12, 3117–3132.

Barnett, T.P., Adam, J.C. and Lettenmaier, D.P. (2005) Potential impacts of a warming climate on water availability in snow-dominated regions. *Nature*, 438, 303–309.

Beniston, M. (2012) Is snow in the Alps receding or disappearing? *Wiley Interdisciplinary Reviews: Climate Change*, 3, 349–358.

Chen, X.N., Bao, A.M. and Liu, P. (2010) Quality assessment of MOD10A1 in the Tianshan Mountains based on multiple statistical sample scales. *Remote Sensing for Land & Resources*, 25, 80–85.

Dettinger, M.D. and Cayan, D.R. (1995) Large-scale atmospheric forcing of recent trends toward early snowmelt runoff in California. *Journal of Climate*, 3, 606–623.

Dietz, A.J., Wohner, C. and Kuenzer, C. (2012) European snow cover characteristics between 2000 and 2011 derived from improved MODIS daily snow cover products. *Remote Sensing*, 4, 2432–2454.

Ding, Y. and Qin, D. (2009) Cryosphere change and global warming: impact and challenges in China. *China Basic Science*, 3, 4–10.

Farr, T.G., Rosen, p.A., Caro, E., Crippen, R., Duren, R., Hensley, S., Kobrick, M., Paller, M., Rodriguez, E., Roth, L., Seal, D., Shaffer, S., Shimada, J., Umland, J., Werner, M., Oskin, M., Burbank, D. and Alsdorf, D. (2007) The shuttle radar topography mission. *Reviews of Geophysics*, 2.

Gao, J., Williams, M.W., Fu, X., Wang, G. and Gong, T. (2012) Spatiotemporal distribution of snow in eastern Tibet and the

response to climate change. *Remote Sensing of Environment*, 121, 1–9.

Guo, L. and Li, L. (2015) Variation of the proportion of precipitation occurring as snow in the Tian Shan Mountains, China. *International Journal of Climatology*, 35, 1379–1393.

Hall, D.K. and Riggs, G.A. (2007) Accuracy assessment of the MODIS snow products. *Hydrological Processes*, 21, 1534–1547.

Hall, D.K., Riggs, G.A. and Salomonson, V.V. (1995) Development of methods for mapping global snow cover using moderate resolution imaging spectroradiometer data. *Remote Sensing of Environment*, 54, 127–140.

Hall, D.K., Riggs, G.A., Salomonson, V.V., DiGirolamo, N.E. and Bayr, K.J. (2002) MODIS snow-cover products. *Remote Sensing of Environment*, 83, 181–194.

Hall, D.K., Salomonson, V.V. and Riggs, G.A. (2016) *MODIS/Terra snow cover daily L3 global 500m grid. Version 6*. Boulder, CO: NASA National Snow and Ice Data Center Distributed Active Archive Center.

Hu, G., Zhao, L., Wu, X., Li, R., Wu, T., Su, Y. and Hao, J. (2019) Evaluation of reanalysis air temperature products in permafrost regions on the Qinghai–Tibetan Plateau. *Theoretical and Applied Climatology*, 138, 1457–1470.

Huang, X., Liang, T., Zhang, X. and Guo, Z. (2011) Validation of MODIS snow cover products using Landsat and ground measurements during the 2001–2005 snow seasons over northern Xinjiang, China. *International Journal of Remote Sensing*, 32, 133–152.

Huang, X., Zhang, X., Li, X. and Liang, T. (2007) Accuracy analysis for MODIS snow products of MOD10A1 and MOD10A2 in northern Xinjiang area. *Journal of Glaciology and Geocryology*, 29, 722–729.

Immerzeel, W.W., van Beek, L.P. and Bierkens, M.F. (2010) Climate change will affect the Asian water towers. *Science*, 328, 1382–1385.

Jiang, P. and Wang, X. (2017) Snow cover extraction method based on the near-infrared band of ETM+ image. *Science of Surveying & Mapping*, 42, 41–46.

Li, C., Su, F., Yang, D., Tong, K., Meng, F. and Kan, B. (2018a) Spatiotemporal variation of snow cover over the Tibetan Plateau based on MODIS snow product, 2001–2014. *International Journal of Climatology*, 38, 708–728.

Li, C., Yan, F., Kang, S., Yan, C., Hu, Z., Chen, P., Gao, S., Zhang, C., He, C., Kaspari, S. and Stubbins, A. (2021) Carbonaceous matter in the atmosphere and glaciers of the Himalayas and the Tibetan Plateau: an investigative review. *Environment International*, 146, 106281.

Li, P. (1988) Preliminary evaluation of seasonal snow resources in China. *Acta Geographica Sinica*, 2, 108–119.

Li, Q., Yang, T., Qi, Z. and Li, L. (2018b) Spatiotemporal variation of snowfall to precipitation ratio and its implication on water resources by a regional climate model over Xinjiang, China. *Water (Basel)*, 10, 1463.

Li, Q., Yang, T., Zhou, H. and Li, L. (2019) Patterns in snow depth maximum and snow cover days during 1961–2015 period in the Tianshan Mountains, Central Asia. *Atmospheric Research*, 228, 14–22.

Li, X., Fu, W., Shen, H., Huang, C. and Zhang, L. (2017) Monitoring snow cover variability (2000–2014) in the Hengduan Mountains based on cloud-removed MODIS products with an adaptive spatio-temporal weighted method. *Journal of Hydrology*, 551, 314–327.

Marke, T., Hanzer, F., Olefs, M. and Strasser, U. (2018) Simulation of past changes in the Austrian snow cover 1948–2009. *Journal of Hydrometeorology*, 19, 1529–1545.

McCabe, G.J. and Wolock, D.M. (2010) Long-term variability in Northern Hemisphere snow cover and associations with warmer winters. *Climatic Change*, 99, 141–153.

Notarnicola, C. (2020) Hotspots of snow cover changes in global mountain regions over 2000–2018. *Remote Sensing of Environment*, 243, 111781.

Paudel, K.P. and Andersen, P. (2011) Monitoring snow cover variability in an agropastoral area in the trans Himalayan region of Nepal using MODIS data with improved cloud removal methodology. *Remote Sensing of Environment*, 115, 1234–1246.

Qin, D., Liu, S. and Li, P. (2006) Snow cover distribution, variability, and response to climate change in western China. *Journal of Climate*, 19, 1820–1833.

Salomonson, V.V. and Appel, I. (2004) Estimating fractional snow cover from MODIS using the normalized difference snow index. *Remote Sensing of Environment*, 89, 351–360.

Schöner, W., Koch, R., Matulla, C., Marty, C. and Tilg, A.M. (2019) Spatiotemporal patterns of snow depth within the Swiss-Austrian Alps for the past half century (1961 to 2012) and linkages to climate change. *International Journal of Climatology*, 39, 1589–1603.

Shan, S., Shen, R., Shi, C., Bai, L. and Sun, S. (2020) Evaluation of land surface temperature and 2 m air temperature from five reanalyses datasets across north China in winter. *Plateau Meteorology*, 39, 37–47.

Shen, Y., Su, H., Wang, G., Mao, W., Wang, S., Han, P., Wang, N. and Li, Z. (2013) The responses of glaciers and snow cover to climate change in Xinjiang (II): hazards effects. *Journal of Glaciology and Geocryology*, 35, 1355–1370.

Tang, Z., Wang, J., Li, H. and Yan, L. (2013) Spatiotemporal changes of snow cover over the Tibetan Plateau based on cloud-removed moderate resolution imaging spectroradiometer fractional snow cover product from 2001 to 2011. *Journal of Applied Remote Sensing*, 7, 73582.

Tang, Z., Wang, X., Wang, J., Wang, X., Li, H. and Jiang, Z. (2017) Spatiotemporal variation of snow cover in Tianshan Mountains, Central Asia, based on cloud-free MODIS fractional snow cover product, 2001–2015. *Remote Sensing*, 9, 1045.

Van De Kerchove, R., Lhermitte, S., Veraverbeke, S. and Goossens, R. (2013) Spatio-temporal variability in remotely sensed land surface temperature, and its relationship with physiographic variables in the Russian Altay Mountains. *International Journal of Applied Earth Observation and Geoinformation*, 20, 4–19.

Wang, H., Zhang, X., Xiao, P., Zhang, K. and Wu, S. (2021) Elevation-dependent response of snow phenology to climate change from a remote sensing perspective: a case survey in the central Tianshan mountains from 2000 to 2019. *International Journal of Climatology*, 42, 1706–1722.

Wang, W., Huang, X., Deng, J., Xie, H. and Liang, T. (2015) Spatio-temporal change of snow cover and its response to climate over the Tibetan Plateau based on an improved daily cloud-free snow cover product. *Remote Sensing*, 7, 169–194.

Wang, X., Xie, H. and Liang, T. (2008) Evaluation of MODIS snow cover and cloud mask and its application in northern Xinjiang, China. *Remote Sensing of Environment*, 112, 1497–1513.

Wang, Y., Li, G. and Zhang, Y. (2011) Regional representativeness analysis of national reference climatological stations based on MODIS/LST product. *Journal of Applied Meteorological Science*, 22, 214–220.

Wu, S., Zhang, X., Du, J., Zhou, X., Tuo, Y., Li, R. and Duan, Z. (2019) The vertical influence of temperature and precipitation on snow cover variability in the central Tianshan Mountains, northwest China. *Hydrological Processes*, 33, 1686–1697.

Wu, X., Shen, Y., Wang, N., Pan, X., Zhang, W., He, J. and Wang, G. (2016) Coupling the WRF model with a temperature index model based on remote sensing for snowmelt simulations in a river basin in the Altay Mountains, north-west China. *Hydrological Processes*, 30, 3967–3977.

Xie, H., Wang, X. and Liang, T. (2009) Development and assessment of combined Terra and Aqua snow cover products in Colorado Plateau, USA and northern Xinjiang, China. *Journal of Applied Remote Sensing*, 3, 33559.

Ye, H. and Mather, J.R. (1997) Polar snow cover changes and global warming. *International Journal of Climatology*, 17, 155–162.

Yi, S., Wang, Q., Chang, L. and Sun, W. (2016) Changes in mountain glaciers, lake levels, and snow coverage in the Tianshan monitored by GRACE, ICESat, Altimetry, and MODIS. *Remote Sensing*, 8, 798.

Zhang, D., Yang, Y. and Lan, B. (2018) Climate variability in the northern and southern Altai Mountains during the past 50 years. *Scientific Reports*, 8, 1–11.

Zhang, W., Kang, S., Shen, Y., He, J. and Chen, A. (2017) Response of snow hydrological processes to a changing climate during 1961 to 2016 in the headwater of Irtysh River Basin, Chinese Altai Mountains. *Journal of Mountain Science*, 14, 2295–2310.

Zhang, X., Xiong, Z. and Yan, X. (2019b) Modeling precipitation changes in the Heihe River Basin, northwest China, from 1980 to 2014 with the regional integrated environment modeling system (RIEMS) nested with ERA-Interim reanalysis data. *Theoretical and Applied Climatology*, 137, 493–503.

Zhang, Y., Kang, S., Gao, T., Schmale, J., Liu, Y., Zhang, W., Guo, J., Du, W., Hu, Z., Cui, X. and Sillanpää, M. (2019a) Dissolved organic carbon in snow cover of the Chinese Altai Mountains, Central Asia: concentrations, sources and light-absorption properties. *Science of the Total Environment*, 647, 1385–1397.

Zhong, X., Kang, S., Zhang, W., Yang, J., Niu, H., Liu, Y., Guo, J., Li, X., Chen, P. and Wang, X. (2021a) Continuously observed light absorbing impurities in snow cover over the southern Altai Mts. in China: concentrations, impacts and potential sources. *Environmental Pollution*, 270, 116234.

Zhong, X., Zhang, T., Su, H., Xiao, X., Wang, S., Hu, Y., Wang, H., Zheng, L., Zhang, W., Xu, M. and Wang, J. (2021b) Impacts of landscape and climatic factors on snow cover in the Altai Mountains, China. *Advances in Climate Change Research*, 12, 95–107.

How to cite this article: Qin, S., Xiao, P., & Zhang, X. (2022). How do snow cover fraction change and respond to climate in Altai Mountains of China? *International Journal of Climatology*, *42*(14), 7213–7227. https://doi.org/10.1002/joc.7640